Energy Conversion and Management: X 24 (2024) 100706

Contents lists available at ScienceDirect

Energy Conversion and Management: X

journal homepage: www.sciencedirect.com/journal/energy-conversion-and-management-x

Methodology to assess the impact of urban vegetation on the energy consumption of residential buildings. Case study in a Mediterranean city

C. Prades-Gil [a,b,*,1], J.D. Viana-Fons [a,b], X. Masip [a,b], A. Cazorla-Marín [a], T. Gómez-Navarro [a]

[a] Institute for Energy Engineering, Universitat Politècnica de València, Camí de Vera s/n, 46022 València, Spain
[b] Grupo ImpactE Planificación Urbana SL, Carrer Pedro Duque, Camí. de Vera, s/n, 46022 València, Spain

ARTICLE INFO

Keywords:
Landsat-8
Nature-based solutions
Heating & Cooling
GIS

ABSTRACT

The global growth of urban areas is unstoppable, and this growth is accompanied by an intensification of urban heat island effects, exacerbating the challenges of climate change and sustainable urban development in warm climates. In this context, understanding the intricate dynamics of these phenomena and their implications on the thermal behaviour of buildings becomes paramount. This study focuses on València, a Spanish city characterized by a Mediterranean climate, where the interplay between ground temperature variations, vegetation levels, and the thermal demands of buildings is investigated.

Land surface temperature measurements derived from satellite data, specifically from the Landsat-8 mission, provide a valuable lens through which to assess the heat island effect. These measurements are harmonized with data collected from local weather stations to establish a robust foundation for evaluating the thermal dynamics of the urban environment. European standards, coupled with Geographic Information System technologies, enable the simulation of temperature variations, and facilitate a nuanced analysis of their impact on the thermal demands of a building.

Moreover, recognizing the crucial role played by the urban climate in the influencing of heating and cooling needs, this study explores nature-based solutions implemented in València. By leveraging satellite-derived temperature and vegetation data over an extended period, it is possible to identify actions and elements that contribute positively to mitigating UHI effects and improving the overall climatic conditions. Results indicate that vegetation has a notable impact on local temperature, with distinct patterns observed in different seasons. The research incorporated the simulation of climate scenarios, introducing varying levels of vegetation. Results demonstrated a substantial reduction in cooling demand, particularly during the summer months. Buildings with a lower exterior surface-to-volume ratio exhibited a more pronounced reduction in energy consumption.

1. Introduction

Climate change is the most significant challenge ever encountered by humanity; several sectors are implicated in its causation [1], and in order to offer a response, it is imperative that all the sectors become involved in comprehensive planning [1]. Cities, responsible for a substantial 72 % of greenhouse gas emissions, are particularly pivotal in this endeavour, especially considering their projected role as hosts to around 70 % of the global population by 2050 [2]. As key battlegrounds against global warming, cities play a crucial role in enhancing the quality of life for their inhabitants [1].

Effective planning for the coming years is crucial to achieving the goals of climate change mitigation and adaptation. In this regard, energy usage emerges as a critical focus point due to its significant environmental impact. Due to their high energy demand resulting from population density, cities in particular come under the spotlight [1]. Planning must extend to regions prone to extreme climates, where quality of life is seriously endangered. Adaptation and mitigation strategies, especially in cities with Mediterranean climates and similar, facing extreme conditions, demand the meticulous examination of microclimates and action plans based on climate change forecasts [3].

Extreme weather events have surged in the last two decades, causing severe heatwaves, intense droughts in Southern Europe, biodiversity loss, and flooding in Central Europe [4]. The outlook is serious if effective measures are not taken. In response, the European Union has

* Corresponding author.
E-mail address: carpragi@upv.edu.es (C. Prades-Gil).
[1] ORCID: 0000-0003-0750-8846.

https://doi.org/10.1016/j.ecmx.2024.100706
Received 19 December 2023; Received in revised form 30 July 2024; Accepted 4 September 2024
Available online 7 September 2024

Nomenclature

LST	Land surface temperature
NDVI	Normalised Difference Vegetation Index
UHI	Urban Heat Island effect
NBS	Nature-based solutions
AMSL	Above mean sea level
RH	Relative humidity
S/V	Shape factor
GIS	Geographic Information Systems
AT	Air Temperature
kWh	kilowatt hour

set ambitious targets, aiming to reduce emissions by 80 % compared to 2019 levels across all sectors [5] by 2050. These goals have progressed over the years, culminating in the pursuit of climate neutrality by 2050 [4]. The European Union's comprehensive action plan focuses on all sectors, with specific attention to cities and buildings. Key objectives include maximizing the benefits of energy efficiency through zero (or positive) energy buildings, the widespread deployment of renewable energy, the promotion of clean and secure mobility, the fostering of a circular economy, the creation of carbon sinks, the implementation of green infrastructure, and advances in carbon capture [4].

As a result, it is necessary to study climate at the local level so as to produce indicators that will help decision-making at the municipal level. In this way, if the neighbourhoods which have the most extreme conditions are known, it will be easier to propose adaptation and mitigation measures and determine where they would have the greatest impact.

Several studies, exemplified by [6], delve into the evaluation of climate change-induced uncertainties in energy dynamics. This research generates diverse future scenarios, emphasizing the importance of climate models considering extreme climates over traditional Typical Meteorological Year (TMY) approaches. Other studies, such as [7], explore the impact of the urban heat island effect on the energy consumption of various buildings in Rome, offering insights into the interconnectedness of climate and energy demand.

In the realm of urban planning, methodologies such as those presented in [8] aim to prioritize impactful actions. The authors propose a methodology for the selection of buildings suitable for green roofs, considering parameters such as the urban heat island effect. Results suggest that green roofs can significantly enhance the urban microclimate, offering multifaceted advantages, including thermal demand reduction, the mitigation of heat islands, poverty alleviation, support for biodiversity, flood prevention, and habitat creation.

An examination into the manifold benefits of nature-based interventions extends to comprehensive studies investigating their impact on local fauna and public health. A significant contribution in this domain is exemplified by [9], which elucidates how green roofs positively affect biodiversity in comparison to traditional roofing structures. Conducted in a municipality near València, a Mediterranean city, the study concludes that vegetated roofs significantly enhance biodiversity, offering valuable insights into the ecological advantages of such interventions in this climatic context. In tandem, a parallel exploration of health implications is undertaken by another notable study, [10]. This analysis investigates the correlation between mortality rates and the Urban Heat Island (UHI) effect, demonstrating how integrating green spaces into urban infrastructure could mitigate the health risks associated with urban heat. These findings underscore the holistic advantages of incorporating nature-based solutions into urban planning, showcasing their potential to positively influence both ecological and human health dynamics.

However, the implementation of nature-based measures requires a nuanced assessment of their diverse effects and their potential to mobilize the population. [11] critically evaluates the societal repercussions of nature-based initiatives, highlighting how renaturalization efforts can inadvertently lead to green gentrification and the displacement of vulnerable communities. This thorough investigation across 28 cities in the Northern Hemisphere underscores the need for strategic policies to counteract potential inequalities stemming from renaturalization, emphasizing that these measures should first and foremost improve the overall quality of life for the existing population.

A research initiative conducted at the University of Florida [12] investigates the nuanced impacts of the Heat Island Effect as regards climatic conditions and its influence on building energy consumption in the United States. The study specifically explores the relationship between UHI and climatic variables, such as Degrees Day, absolute humidity, and solar radiation, revealing a direct correlation. Notably, wind speed and precipitation exhibited no discernible impact while the absolute humidity of the city enhanced the effect of UHI on building energy demand. The findings indicate that UHI contributes to heightened energy demand in warmer regions while conversely reducing demand in colder areas. This underscores the contextual dependence of the phenomenon on specific climatic variables, highlighting that its effects are not universally applicable across temperate climate zones. In regions characterized by warm climates, the lengthening of the summer period due to climate change emerges as a critical health concern for inhabitants. The urban heat island effect further exacerbates this challenge, as metropolitan temperatures surpass those of surrounding areas owing to human activities, building materials, and urban traffic. While the literature offers an extensive examination of the assessment of the heat island effect, the modification it induces in the thermal demand of buildings has received comparatively little attention. Recognizing the significance of this relationship, especially in warm climates, is crucial for effective urban energy planning.

It should be noted that UHI cannot be generalized to a single parameter. Researchers must delve into the complex interplay of variables influencing localized temperature increases in order to comprehend the factors that make a significant contribution to urban hot spots. This has been the subject of much research and a comprehensive examination of the urban heat island (UHI) phenomenon, and its contributing factors can be found in [13]. Additionally, studies such as [14] shed light on the intricate dynamics of urban microclimates, offering valuable insights into the specific factors that contribute to the formation and intensification of hot spots within urban environments. Atmospheric turbulence emerges as a critical factor, influencing air mixing and subsequently impacting local temperatures. Research into the energy exchanges between urban surfaces and the surrounding atmosphere provides insights into the heat accumulation dynamics within urban areas. Land use composition, including the prevalence of impervious surfaces, buildings, and green spaces, plays a pivotal role in UHI generation. The presence and characteristics of urban vegetation directly influence solar radiation absorption and evaporation, further modulating temperature patterns. Additionally, the choice of construction materials contributes significantly, with materials possessing high thermal inertia influencing local heat retention. Finally, anthropogenic activities, particularly vehicular traffic and industrial processes, contribute substantial heat emissions, amplifying the UHI effect. This multifaceted examination underscores the intricate interplay of these factors in shaping the urban thermal environment [14].

Nature-based solutions (NBS) have gained popularity as an effective means of reducing energy demand and mitigating the impacts of climate change in urban environments. The integration of green infrastructure, such as urban parks, green roofs, and vertical gardens, can help to reduce urban heat island effects, lower the demand for energy-intensive heating and cooling, and promote energy conservation [15]. Urban parks are a key component of NBS that can help to reduce energy demand in cities. Research by Konarska [16] showed that the presence of urban parks can reduce cooling demand by up to 40 % during peak summer months. Moreover, the use of urban parks can promote energy

conservation by reducing the need for energy-intensive indoor activities, such as exercising and socializing. Research by Wahba et al. [17] showed that the implementation of green roofs and walls can also reduce the cooling demand of a building by up to 25 %. Similarly, green facades have been shown to reduce the surface temperature of buildings by up to 9 °C [18], while Davis et al. [19] demonstrated that the implementation of vertical gardens on building facades can reduce the cooling demand of a building by up to 8 %.

It is essential to monitor vegetation levels in cities for the purposes of understanding urban green spaces, their distribution, and changes over time. Satellite imagery provides a valuable tool for the assessment of vegetation cover and density in urban environments. Sari et al. [20] employed high-resolution satellite images to assess vegetation cover in a rapidly expanding city. They found that urban areas with higher vegetation cover exhibited lower surface temperatures and reduced energy consumption. Satellite imagery also allows for temporal analysis, enabling researchers to monitor changes in vegetation levels over time. For example, Özyavuz [21] made use of multi-temporal satellite images to investigate vegetation trends in urban parks, highlighting the importance of vegetation maintenance and management to sustain healthy green spaces. His findings demonstrated the effectiveness of satellite-based monitoring in quantifying changes in vegetation cover and identifying areas with decreasing green spaces.

Vegetation indices are commonly used to assess vegetation levels in urban areas using satellite imagery. The most widely-used vegetation index is the Normalized Difference Vegetation Index (NDVI), which measures the amount of green vegetation in an area. Research by Khalifa et al. [22] shows that NDVI can accurately capture changes in vegetation cover over time. Moreover, the use of additional vegetation indices, such as the Enhanced Vegetation Index (EVI) and the Green Normalized Difference Vegetation Index (GNDVI), can provide a more comprehensive understanding of vegetation cover and composition in urban areas [23].

While satellite imagery provides a powerful tool for assessing vegetation levels in urban areas, there are some challenges that need to be addressed. One challenge is the presence of shadows and built-up areas, which can interfere with the accuracy of vegetation measurements. Research by Chen et al. [24] demonstrated that the use of high-resolution imagery and advanced image processing techniques can help to mitigate these challenges, resulting in more accurate assessments of vegetation levels in urban areas.

On the other hand, surface temperature is an important indicator of urban heat island effects [25]. Satellite imagery also provides accurate means of assessing surface temperature in urban areas [26]. Recent advances in remote sensing technology have enabled the collection of high-resolution imagery, which can capture detailed information on surface temperature at a fine spatial scale; for example, research by Kim et al. [27] showed that satellite imagery can accurately measure surface temperature in urban areas, with an accuracy of up to 90 %.

The most widely-used thermal index to assess surface temperature in urban areas using satellite imagery is the Land Surface Temperature (LST). LST measures the radiative temperature of the land surface. Research by Yang et al. [28] showed that LST can accurately capture changes in surface temperature in urban areas over time. Moreover, the use of additional thermal indices, such as the Surface Urban Heat Island Intensity (SUHII) and the Urban Heat Island Effect (UHIE) index, can provide a more comprehensive understanding of surface temperature in urban areas.

Assessing surface temperature in urban areas with satellite imagery also has some challenges that need to be addressed. The main one is the presence of atmospheric effects, which can interfere with the accuracy of temperature measurements. Research by Tan et al. [29] demonstrated that the use of advanced image processing techniques, such as atmospheric correction and emissivity estimation, can help to mitigate these challenges, resulting in more accurate assessments of surface temperature in urban areas.

In this paper, the authors have considered the use of Landsat-8 satellite imagery based on a thorough review of the existing literature, in particular reviews elucidating various methodologies for the study of urban microclimates. One noteworthy review, comprehensively covering models applicable to urban climate studies, is presented by [30]. The review emphasizes the multifaceted nature of urban climate modelling, necessitating diverse data sets and processing techniques. Parameters crucial for Urban Climate Models (UCMs) are categorized into land use/land cover classes, morphological information, architectural details, socio-economic parameters, and urban vegetation description. Additionally, the review by [31] focuses on numerical models for thermal analysis at mesoscale and microscale in mid-latitude climate regions. This study classifies tools and models based on their resolution and usage, providing a nuanced understanding of their pros and cons.

Considering the resolution and applicability of different models, satellite imagery, especially Landsat-8, emerges as a valuable tool for mesoscale studies. The Landsat-8 satellite offers a global coverage with high spatial resolution, around 100 m for temperature, making it particularly suited for observing Urban Heat Island (UHI) dynamics. Although its temporal resolution is comparatively low, and interference from cloud cover is a limitation, the real-world results derived from satellite imagery provide a tangible advantage over model-generated outcomes [31].

The decision to focus on Landsat-8 is underscored by specific studies such as the analysis conducted in Skopje, Macedonia [32], which provides foundational insights into UHI patterns. Moreover, investigations in Santiago, Chile [33], exemplify the satellite's capacity to capture spatio-temporal variations in UHI, leveraging its thermal bands. Notably, studies such as the piece comparing land surface and air temperatures in a snow climate city [34] showcase Landsat-8′s effectiveness by demonstrating statistically significant relationships between Land Surface Temperature (LST) and Air Temperature (AT). The study affirms that LST is a considerably stronger indicator of Surface Urban Heat Island (SUHI) intensity than AT, both in summer and winter, providing valuable data for understanding UHI dynamics.

2. Objectives and innovation

This paper presents a methodology for the evaluation of the potential effect on the thermal demand of buildings of increasing the vegetation level of urban areas affected by the Heat Island effect. For this purpose, real measurements from satellite and weather stations are used. Firstly, vegetation indexes and land surface temperatures are extracted from satellite images of the urban area to obtain a correlation between these two variables. Secondly, the land surface temperature is compared with measurements from weather stations around the city, obtaining a second correlation. With these correlations, it is possible to calculate the fall in the air temperature caused by an increase in the vegetation level. Finally, the air temperature of a weather file is modified accordingly to calculate the thermal demand of the buildings, i.e. including the effect of the vegetation. The methodology is applied to several districts of the city of València, considering the construction typologies presented in the city. Thus, the research had the following objectives:

- To obtain the vegetation index and land surface temperature for the city of València.
- To evaluate the relationship between the vegetation index and land surface and air temperatures.
- To estimate the effect of increasing the vegetation index on the air temperature.
- To calculate the impact of increasing the vegetation index on the thermal demand of the buildings.

This way, the paper proposes the following contributions:

- To propose a methodology to adapt a weather file considering the effect of increasing the vegetation index.
- To evaluate the change in the thermal demand of buildings in urban areas when a nature-based solution is implemented.

3. Materials

3.1. Study area

València (39.46962, −0.37636), situated on the eastern coast of the Iberian Peninsula on the Mediterranean Sea, is the third most populous city in Spain, Europe. Encompassing an area of 134.65 km2, València experiences a mild and slightly rainy Mediterranean climate during winters, transitioning to hot and dry conditions in the summers. According to Köppen's climate classification criteria, the climate of València transitions between Mediterranean (Csa) and warm semi-arid (BSh), with an average annual temperature of 18.4 °C [35].

València 's climate manifests warm summers and mild winters, with January being the coldest month, featuring average maximum temperatures of 16–17 °C and minimum temperatures of 7–8 °C. In contrast, August emerges as the warmest month, characterized by average maximum temperatures of 30–31 °C, minimum temperatures of 21–23 °C, and moderately high absolute humidity. The daily thermal amplitude remains limited, averaging around 9 °C, attributed to maritime influences. Similarly, the annual thermal amplitude remains modest, ranging between 9 and 10 °C, influenced by the proximity of the sea [35].

Fig. 1 shows land use, differentiating between vegetation and crops (light green), water bodies (blue), and any type of construction or land use as buildings or roads (red). Data obtained from the Valencian Cartographic Institute [36]. As can be seen in Fig. 1, the city of Valencia is surrounded by a wide plain, is on the coast and is not too urbanised around it. However, due to its intrinsic urbanism, the intense activity in the city and climate change, the UHI effect is noticeable, as discussed throughout this article.

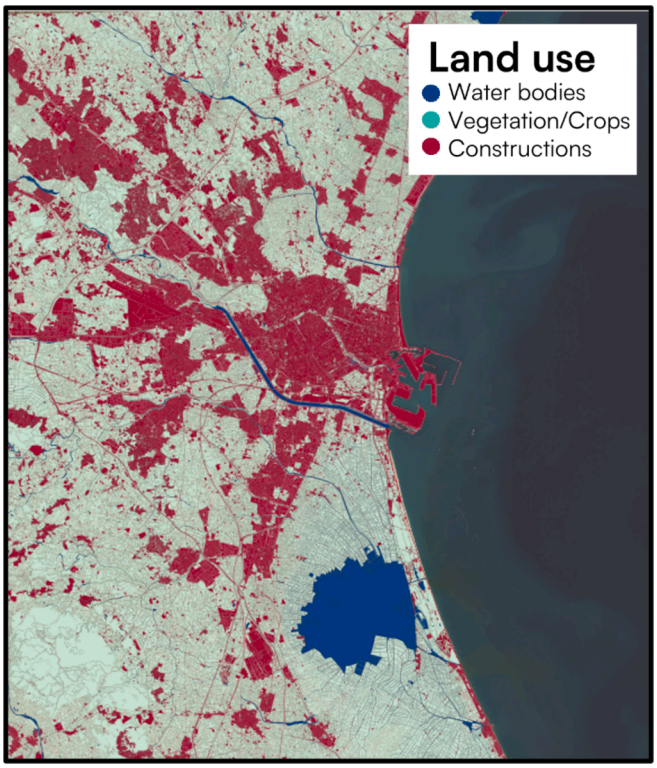

Fig. 1. Land use of València and its surroundings.

Annual precipitation in València ranges from 450 to 500 mm, with pronounced minima during the summer months (June to August), notably in July, averaging around 8 mm. In contrast, the autumn months, particularly September and October, experience maxima, with October reaching slightly below 80 mm on average. The annual average humidity remains relatively high, between 9 and 15 g/m^{3,} exhibiting minimal variation throughout the year due to the maritime influence [35].

The districts of the urban centre of València have been chosen for the case study. Fig. 2 shows their spatial organisation. The districts are: Ciutat Vella, Eixample, Extramurs, Campanar, La Saïdia, El Pla Del real, Benimaclet, Rascanya and Benicalap. Only these districts were chosen in order to decrease the effect of big water masses, such as the Mediterranean Sea, located to the east, the River Turia to the south and the "Albufera" Lake to the far south. Therefore, the effect of vegetation on temperature is studied in the most heavily urbanised areas of the city.

3.2. Data sources

3.2.1. Acquisition of satellite images – Landsat-8

The datasets used in the article comprise Landsat-8 satellite images, climatic files collected from various installations across the city, and geo-spatial information for constructing 3D models of buildings. Landsat-8 satellite images have a spatial resolution of 30 m for bands 1 to 9 (except for band 8, which has 15-m resolution) and a 100-meter spatial resolution for the infrared or TIRS bands, from 10 to 11. The images date from the years 2014, 2015, 2019, 2020, 2021, 2022 and 2023. The specific dates are shown in Table 3. On the data acquisition dates, the sky conditions were clear. All the images were captured at around 10:00 a.m. local time due to the limited availability and suitability of Landsat 8 TIRS. Before interpretation and LST retrievals, radiometric correction and co-registration processes were applied to these images, ensuring their correction to the UTM projection system.

3.2.2. Climate files from weather stations

The authors have also made use of measurements from several weather stations located throughout the city of València, that can be consulted in Fig. 3. Information regarding the distribution, location, dates, height above mean sea level (AMSL) and distance from the sea, is given in Table 1. The information has been provided by the Valencian meteorological association AVAMET [37] and the national Spanish meteorological Agency AEMET [38]. All the weather stations are made of professional calibrated equipment and are installed at several meters above the ground level. The location of the stations can be consulted in Fig. 3.

4. Methodology

In this section, the methodology employed in the current study is detailed. The workflow of the methodology can be seen in Fig. 4. The steps undertaken in the methodology are the following:

1. Relation between LST and NDVI. Acquisition from satellite images.
2. Relation between AT and LST.
3. New scenarios based on NDVI increments, improved weather files & thermal demand simulation.

4.1. Relationship between LST and NDVI. Acquisition from satellite images

Landsat-8 mission data is used to obtain the values of NDVI and LST at the different locations of the city; this is because of its high spatial resolution in comparison with other typical satellites that have low spatial resolution but higher temporal resolution: for example, MODIS [33]. Landsat-8 [39] pictures allow the study of temperatures and

Fig. 2. Area under study in the city of València, Spain, Europe.

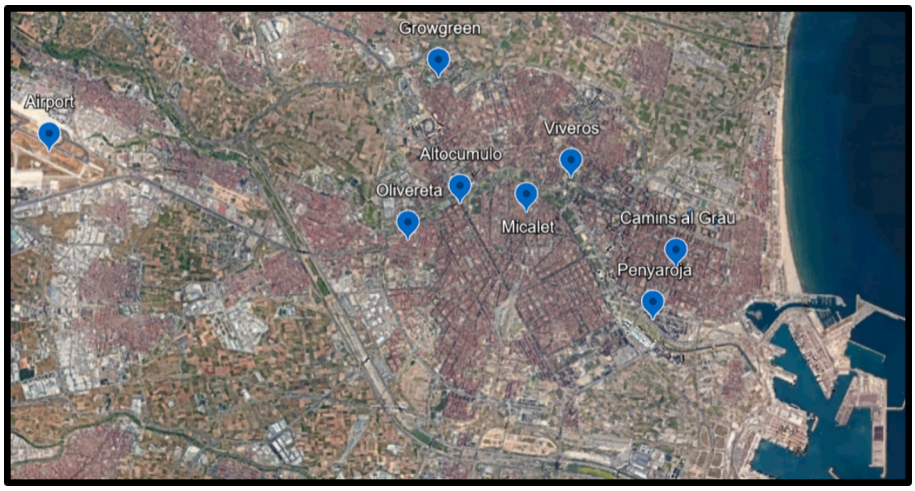

Fig. 3. Locations of weather stations.

Table 1
Information related the weather stations.

Station	Source	Type	Lon	Lat	Height AMSL	Distance from sea	First date	Last date
Viveros	AEMET	Park	−0.366387	39.480556	11 m	3.9 km	01/01/2020	31/12/2020
Airport	AEMET	Airport	−0.474677	39.485016	56 m	13.1 km	01/01/2020	31/12/2020
Growgreen Benicalap	AEMET	Park	−0.39449	39.49676	22 m	6.4 km	09/01/2019	19/12/2021
Camins al Grau	AVAEMET	Building	−0.3455	39.4666	6 m	2.1 km	01/01/2020	31/12/2021
Olivereta	AVAEMET	Building	−0.4008	39.471	19 m	6.7 km	02/12/2020	31/12/2021
Altocumulo	AVAEMET	Building	−0.390072	39.476774	19 m	5.7 km	01/01/2020	31/12/2021
Micalet	AVAEMET	Building	−0.376359	39.475452	14 m	4.5 km	01/01/2020	31/12/2021
Penyaroja	AVAEMET	Building	−0.350283	39.458332	7 m	1.8 km	01/01/2020	31/12/2021

vegetation indexes inside the city and compare data from different districts, and furthermore, it incorporates data from recent years. The process described below can be consulted in many other studies, such as [34,40] or [40].

For the purposes of calculating NDVI (Normalized Difference Vegetation Index) using bands 4 and 5, it is necessary to use the spectral information from these bands, where band 4 corresponds to the red spectrum, and band 5 corresponds to the near-infrared spectrum. The data has a resolution of 30 m.

$$NDVI = \frac{band_5 - band_4}{band_5 + band_4} \quad (1)$$

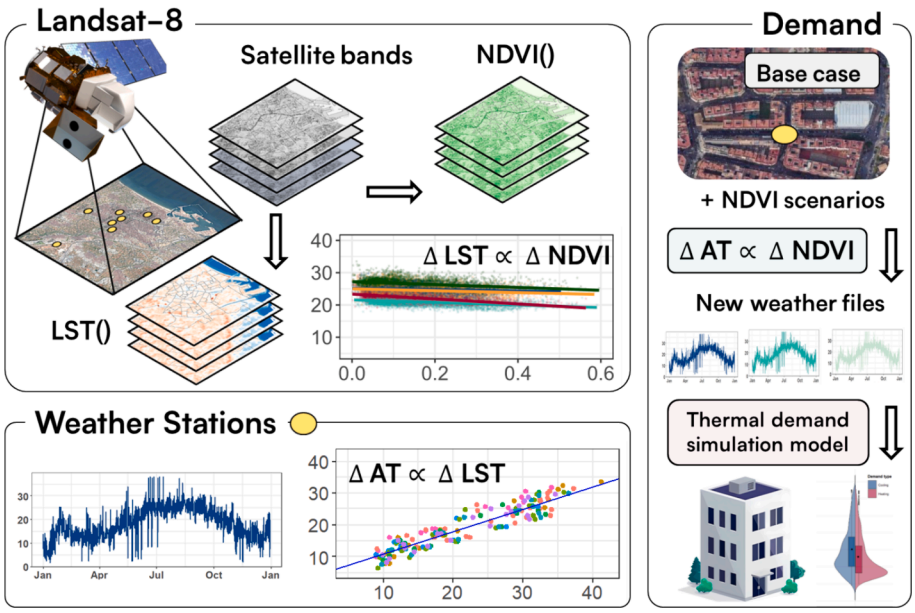

Fig. 4. Visual methodology.

Bands 10 and 11 are employed to calculate the LST,. These bands represent the thermal infrared spectrum and have a resolution of 100 m. Firstly, the Landsat-8 TIRS digital band 10 (DN) is converted to spectral radiance, using the radiance scaling factors provided in the metadata of each image. According to the Data USERS HANDBOOK [41].

$$L_{\lambda 10} = M_L{}^{*} band_{10} + A_L \tag{2}$$

where $L_{\lambda 10}$ is the spectral radiance $\frac{W}{m^{2}{}^{*}sr{}^{*}nm}$ and M_L and A_L are the scaling factors, both parameters provided in the metadata of the image; $band_{10}$, is the satellite band, and the calculation is performed in each pixel value in the image, both for band 10 and band 11. The spectral radiance is thereafter converted into a brightness temperature under an assumption of unity emissivity as follows:

$$T_{b10} = \frac{K_2}{\log\left(\frac{K_1}{L_{\lambda 10}} + 1\right)} \tag{3}$$

T_{b10} is the pixel brightness temperature, K_1 and K_2 are the conversion constants, also provided in the metadata. Finally, to obtain the LST, the brightness temperature should be further corrected based on the land surface emissivity.

$$T_{s10} = \frac{T_{b10}}{1 + \left(\frac{\lambda {}^{*} T_{b10}}{\rho}\right)\log(LSE_{10})} \tag{4}$$

where T_{s10} is the LST(K), λ is the wavelength of radiation emission ($10.9{}^{*}10^{-6}\mu m$); ρ is $1.43{}^{*}10^{-2} mK$; LSE_{10} is land surface emissivity, which can be calculated based on the NDVI threshold method ($e_{s10} = 0.971$, $e_{v10} = 0.987$, $e_{s11} = 0.977$, $e_{v11} = 0.989$).

$$LSE_{10} = e_{s10}{}^{*}(1 - P_v) + e_{v10}{}^{*} P_v \tag{5}$$

NDVI is necessary to obtain the LSE_{10}, being $NDVI_{min}$ and $NDVI_{max}$, which conventionally are 0.2 and 0.5, respectively; the P_v is calculated as follows:

$$P_v = \left(\frac{NDVI - NDVI_{min}}{NDVI_{max} - NDVI_{min}}\right)^2 \tag{6}$$

Finally, a pixel-by-pixel comparison was carried out across every satellite image to examine the correlation between LST and NDVI levels. This made it possible to investigate the impact of vegetation on land surface temperature.

This relationship was studied on a monthly basis so as to assess the impact of vegetation throughout the year. Graphs were generated for each month, aggregating every image sharing the same month but differing as to the dates (days and years). These graphs facilitate the exploration of the relationship between LST and NDVI for each image, as well as for all the images within each month.

A noteworthy observation is the similarity in the slopes formed by images of the same month, as evident in the results section. For each image, the correlation slope between NDVI and LST was recorded, and subsequently, the median was calculated for each month. This process yielded a representative value for the **Δ LST∝Δ NDVI** relationship for each month throughout the year.

4.2. Correlation between AT and LST

Having established the relationship between Land Surface Temperature (LST) and Normalized Difference Vegetation Index (NDVI), the authors aim to ascertain the correlation between LST and Air Temperature (AT). Notably, satellite images exhibit high spatial resolution but low temporal resolution, while climatic data files present null spatial resolution but high temporal resolution. In this section, a comparative analysis of both datasets is conducted to elucidate the relationship between these two terms.

To achieve this, temperature values are obtained for each weather station at the time of satellite image acquisition. Simultaneously, the LST is extracted for the coordinates corresponding to the measurement stations. Consequently, temperature values from both sources are obtained for the same moment and location, facilitating an exploration of the relationship **Δ AT ∝Δ LST.**

Up to this point, the study has revealed the connection between vegetation and ground temperature, as well as the correlation between ground temperature and air temperature. This understanding sets the stage for extrapolating the subsequent relationship, revealing how air temperature is influenced by variations in vegetation levels, **Δ AT ∝Δ NDVI.**

4.3. New scenarios based on NDVI increments, modified climatic data files & thermal demand simulation

Upon establishing the relationships, the subsequent step in the methodology involves selecting a study area and applying new vegetation conditions. Initially, an area of the city is chosen and its LST and NDVI values are obtained for the whole year. Following a similar structure, the median of all satellite-derived measurements is computed for each month, forming the foundational information for creating new scenarios. This baseline scenario is used to compare NDVI increments.

Armed with information from the study area (LST and NDVI), a series of scenarios with varying vegetation levels is proposed. The increase in vegetation levels triggers a change in the zone's LST, which, in turn, can be translated into a change in the location's air temperature. Adjustments are made to the climatic data files using the AT increment derived from the NDVI increase.

The authors adopt an approach based on monthly medians, incorporating the obtained AT increment into all hourly entries of the climatic data file. This process is repeated for each month, effectively modifying the climatic files to reflect the anticipated changes in AT resulting from the increase in NDVI. Once the new scenarios with their respective climatic data files are obtained, the final step involves simulating the thermal demand. The simulation methodology for thermal demand is based on the approach presented in a previous article [42], which follows the European methodology for the calculation of thermal needs [43], both for heating and cooling. This methodology enables the simulation of a substantial number of buildings in condensed time periods, making parametric studies feasible for large scenarios and building combinations. The current study's methodology uses national sources for creating a 3D model of the city and the buildings under investigation, with Geographic Information System (GIS) tools employed for data acquisition and manipulation.

This methodology conducts a detailed analysis of the radiation incident on each surface. The constructive information of the buildings can be modified, and for this purpose, the Tabula project [44] is employed for information on enclosures and characteristics of the city's buildings. The article also outlines a methodology for selecting the study sample, wherein 1000 buildings from the city of València are chosen by neighbourhoods (approximately 50 buildings per neighbourhood), organized by constructive typologies, years and shapes. The more representative a typology, the more instances of that typology are included in the sample.

The buildings used in the study have been simulated with constructive information, the distribution and shape of buildings, a detailed radiation evaluation, and the new climatic data files. In this study, all 1000 buildings have been simulated for the four presented scenarios, which is the same sample as [42]. The constructive information of the buildings used in article [42] is attached in Annex C. As the objective is to understand how changes in climatic conditions would impact each building, the authors examine how alterations in vegetation (and consequently in the climatic data file) would affect each building, considering their unique constructive and formative conditions.

Finally, the thermal demand for heating and cooling is converted into electricity consumption for the purposes of being able to account for the global energy needs, which is calculated by using a heat pump. The efficiencies employed for the study are denoted as 3.7 (Coefficient of Performance: COP) for heating and 5.35 for cooling (Seasonal energy efficiency ratio: SEER). An average seasonal value for the heat pump is selected from [45].

5. Results & discussion

In this section, the results of the study are discussed. As mentioned earlier, the study area is in the city centre of València, and Landsat-8 satellite data has been obtained for this location. The dates of the acquired images can be found in Table 3. Details of the locations where climatic data files were collected are available in Table 1. As regards the building sample under study, it aligns with that of article [42]. A total of 1000 buildings have been simulated under various conditions corresponding to the newly created scenarios.

5.1. NDVI and LST correlations

In this study, the monthly NDVI and LST indices have been obtained for several years, both of which have been compared and an example can be consulted in Fig. 5. In Annex B: NDVI and LST comparison graphs can be consulted: one graph for each month of the year. Due to cloud shadows, it has not been possible to obtain the same number of valid images for every month. Therefore, there is a variable count in each of the graphs.

The information has been presented as follows: each of the graphs represents one month of the year. Data from different years have been represented in each graph. Each colour represents a satellite image on a different day (and in different years). Each point represents a square with a resolution of 100x100 meters, from which the NDVI and LST have been obtained. In this way, the temperature in each area can be compared versus its level of vegetation. For each cloud of points (representing one day of a year), its trend line has been drawn (in the same colour).

From the graphs, it can be seen that the point clouds do not coincide every month, and nor do the trend lines. But it is revealing to note that the slope of the trend lines in each month is practically identical. The difference is seen in the average temperature of the city, which changes on the different dates. Therefore, it is not possible to determine the exact LST based on the NDVI, but it is possible to estimate how the LST is going to decrease when the vegetation level is increased in one specific location, using the correlation slope as a function of the NDVI to predict LST. However, it is not feasible to obtain a correlation on an annual basis since significant differences occur within the months.

The first conclusion extracted from the previous figure is that the average temperature is different, which may be attributed to various atmospheric phenomena, such as the thermal inertia of previous days, the orientation of the predominant wind, etc. Fig. 6 shows the distribution of slopes for every month of the year and their median. The annexed graphs demonstrate how vegetation affects soil temperature, and it may be seen that, vegetation manages to reduce ground temperature during the summer months: the warmer the month, the greater the cooling effect of vegetation. It could, therefore, be inferred that vegetation has a cooling effect on soil temperature. However, it is noteworthy that in the winter months, vegetation even manages to retain the warmth, i.e. to raise the temperature of the area, indicating a positive year-long effect: it reduces temperature in the summer months and increases it (albeit slightly) in the winter months.

The graphs also reveal variations in daily average temperature and changes in trends, which will be the subject of future studies in order to gain a better understanding of how vegetation affects soil temperature. Fig. 6 shows the relationship between NDVI and LST for each satellite image, represented with a boxplot to assess its variability throughout the months of the year. Some months, such as May, exhibit a much more pronounced dispersion. This is possibly due to a change in the trend from positive to negative (in terms of LST reduction by NDVI), whereas in October the trend is reversed.

Thus, the authors have chosen to use the median of the slopes of the correlations between LST and NDVI as the ratio by which an increase in NDVI will affect LST. The proportions used in the study can be found in the following equations (7). A ratio has been generated for each month, and this has been applied to assess how vegetation modifies ground temperature when an increment is applied to the baseline case.

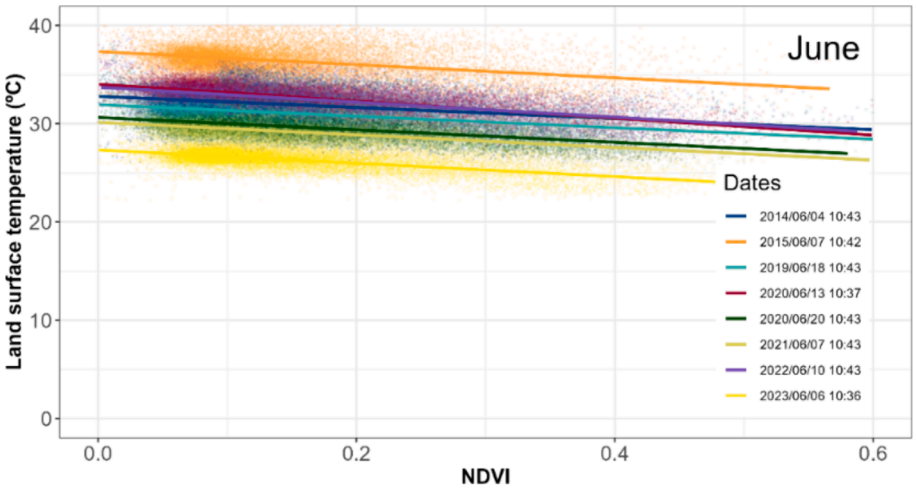

Fig. 5. Relationship between LST and NDVI, for every image of July. Each point represents a pixel.

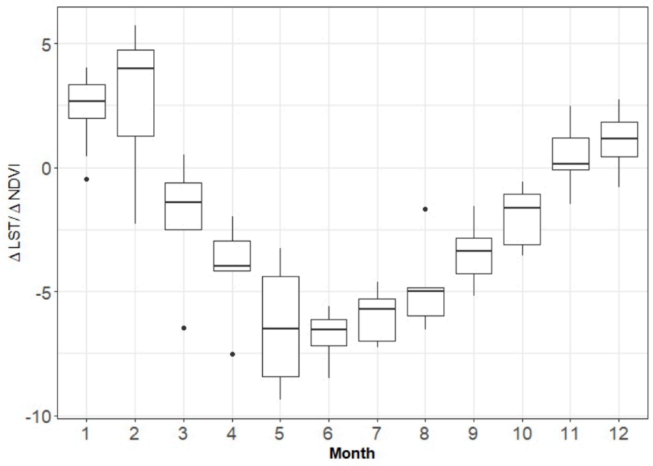

Fig. 6. Collection of slopes of every linear correlation between LST and NDVI for every month.

$$\begin{aligned}
\Delta LST(January) &= 2.68\hat{A}\cdot\Delta NDVI \\
\Delta LST(February) &= 4\hat{A}\cdot\Delta NDVI \\
\Delta LST(March) &= -1.42\hat{A}\cdot\Delta NDVI \\
\Delta LST(April) &= -3.98\hat{A}\cdot\Delta NDVI \\
\Delta LST(May) &= -6.51\hat{A}\cdot\Delta NDVI \\
\Delta LST(June) &= -6.52\hat{A}\cdot\Delta NDVI \\
\Delta LST(July) &= -5.70\hat{A}\cdot\Delta NDVI \\
\Delta LST(August) &= -5.00\hat{A}\cdot\Delta NDVI \\
\Delta LST(September) &= -3.39\hat{A}\cdot\Delta NDVI \\
\Delta LST(October) &= -1.64\hat{A}\cdot\Delta NDVI \\
\Delta LST(November) &= 0.12\hat{A}\cdot\Delta NDVI \\
\Delta LST(December) &= 1.17\hat{A}\cdot\Delta NDVI
\end{aligned} \tag{7}$$

5.2. AT and LST correlations

This section presents the relationship between LST obtained from satellite imagery and AT from climatic stations and, for comparison purposes, the hours from the climatic data file that matched the satellite images were selected. Fig. 7 illustrates this relationship, with each point on the graph representing the combination of existing data from both satellite images and climatic files. Each colour corresponds to a different weather station, distributed throughout the city of València, and the linear correlation for each station has been presented in the same colour as the points for that station. Finally, a general correlation, depicted in blue and extending across the entire graph, has been obtained based on the median of each station's correlations. The equation for the general correlation is provided in the upper-left hand corner of the graph.

In the figure, it is evident that there is a close relationship between

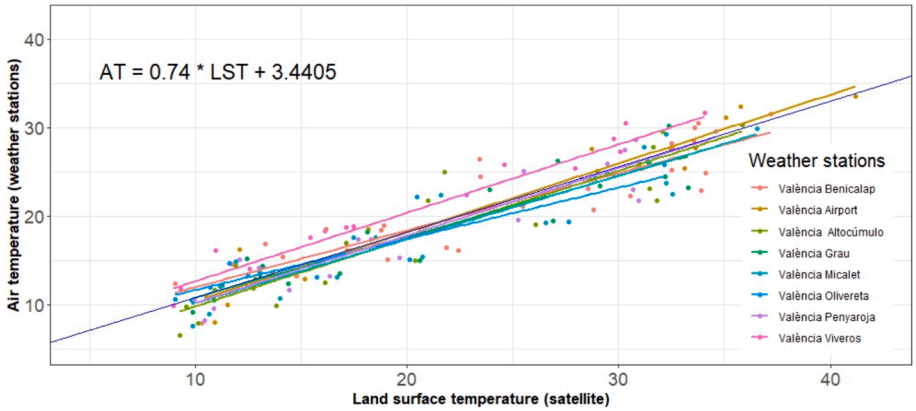

Fig. 7. Relationship between LST and AT, grouped by weather stations, and its correlation.

both parameters, as expected. Notably, as LST increases, the rise in AT is less pronounced. Numerous other writers have noted [33] that the relationship between AT and LST is significant and varies throughout the whole range. During the summer, the air temperature is typically lower than the LST. Another publication that shows a similar effect is [34], in which the study is conducted in a snowy Chinese city where summertime low temperatures are higher than wintertime lows.

It is important to note that the measurement station captures the temperature at a specific point, whereas the satellite image provides information for a 100x100 meter tile. Naturally, the temperature measured by the satellite image takes into account various factors in the image area, resulting in dispersion relative to air temperature. This comparison and the subsequent use of correlations have been conducted from a qualitative standpoint. The authors do not aim to predict air temperature based on ground temperature. The goal of this comparison is to understand how a change in LST might be expected to influence AT.

So, as an example, if the LST of zone A is 30 °C, the AT of zone A is 27 °C and in the new scenario for zone A (called A') the LST of zone A' is 28 °C, the process to estimate the AT of zone A', is:

$$AT_{A'} = AT_A - (AT(LST_A) - AT(LST_{A'})) \tag{8}$$

$$AT_{A'} = 27^{\circ}C - (AT(30^{\circ}C) - AT(28^{\circ}C)) = 27 - (25.6405 - 24.1605) = 25.52^{\circ}C \tag{9}$$

5.3. Generation of new scenarios

The next step involves the generation of new scenarios for the case study; as a means of testing the methodology, the Olivereta station has been used, about which there is more information available in Table 1. This station is located at coordinates 39.471, 0.4008 and is characterized by the absence of virtually any vegetation in the area. Table 2 provides the median values of LST and NDVI for each month (derived from every satellite image in the study).

At this location, the authors have increased vegetation levels in three scenarios. A low-density scenario, where 0.15 has been added to the NDVI for each month; a medium-density scenario with an NDVI increase of 0.3, and a high-density vegetation scenario where the NDVI has been increased by a value of 0.45. Various points in the city with different vegetation indices were studied in order to make this decision. A constant value was added every month to maintain the variability of the NDVI already present in the study area. Given the methodology, any NDVI distribution could be chosen for each month of the year, and with this NDVI increment hypothesis, the authors aim to test the proposed methodology, without claiming that it reflects the distribution resulting from nature-based solutions. Defining the NDVI distribution by month will be the subject of future analysis. Table 2 displays the three scenarios along with the results for each month. With the new NDVI values, the expected increase in LST in that area has been calculated. Similarly, the increase in LST using the equations outlined in the study allows conversion into an increase in AT.

As a visual aid, Fig. 8 illustrates the increase in AT for each month and scenario. It is noteworthy that, for the summer months, a significant reduction in air temperature can be observed, while for the winter months, there is a less pronounced increase. The months of spring and autumn show values close to zero, with an imperceptible effect on temperature. This result is similar to those found in the literature [16,46]. This monthly increment curve will be added to the climatic data file for the study area, specifically the Olivereta weather station. The climatic data file will be supplemented with the increase for every hour of the month, adding the respective increment for each month accordingly.

5.4. Thermal demand and consumption results

Once the new climatic data files for each scenario have been generated, the next step was the simulation of the thermal demand for buildings. Through simulation, the expected heating and cooling thermal demand for each building in each scenario will be determined. This enables the assessment of the potential reduction that nature-based solutions could contribute to the study area. The methodology followed aligns with that presented in [42], simulating the same sample of buildings from that study. A total of 1000 buildings from across the city of València were simulated for the four scenarios: base, low increase, medium increase, and high increase. All of the buildings were simulated as if they were in the same area of the city in which the Olivereta weather station is located. This approach was chosen to observe the variability of results with the aim of exploring whether nature-based measures affect all buildings to the same extent. These questions will be addressed through subsequent graphs.

The first results graph is Fig. 9. This figure presents the thermal demand for heating and cooling for every building and each month. The graph is a box plot illustrating the distribution of normalized thermal demand per unit area (kWh/m2). To complement this information, Fig. 10 displays the distribution of annual demand for every building across all the studied scenarios and shows an evident reduction in cooling demand as well as a drop, although to a lesser extent in heating demand. The distribution of the four scenarios is quite similar, but it is possible to observe a higher concentration of cases around 15–20 kWh/m^2. It could be inferred that these measures have had a greater impact on some buildings with higher demands than on others.

5.5. Consumption savings due to vegetation

Now that the electricity consumption for each building and scenario is available, the impact of nature-based measures has been calculated. Thus, for each scenario, the simulation result has been subtracted from

Table 2
Base case and information on new NDVI scenarios.

	Base		Low NDVI increase ΔNDVI = 0.15		Mid NDVI increase ΔNDVI = 0.3		High NDVI increase ΔNDVI = 0.45	
Month	NDVI	LST	ΔLST	ΔAT	ΔLST	ΔAT	ΔLST	ΔAT
1	0.031	10.277	0.402	0.298	0.805	0.595	1.207	0.893
2	0.042	13.508	0.600	0.444	1.199	0.888	1.799	1.331
3	0.066	20.682	−0.212	−0.157	−0.425	−0.314	−0.637	−0.471
4	0.090	23.561	−0.597	−0.442	−1.194	−0.884	−1.791	−1.326
5	0.086	28.967	−0.977	−0.723	−1.954	−1.446	−2.931	−2.169
6	0.091	32.794	−0.979	−0.724	−1.958	−1.449	−2.936	−2.173
7	0.085	33.377	−0.856	−0.633	−1.712	−1.267	−2.567	−1.900
8	0.078	32.186	−0.750	−0.555	−1.500	−1.110	−2.250	−1.665
9	0.071	25.756	−0.508	−0.376	−1.017	−0.752	−1.525	−1.129
10	0.061	23.289	−0.245	−0.182	−0.491	−0.363	−0.736	−0.545
11	0.040	15.718	0.018	0.013	0.036	0.027	0.054	0.040
12	0.033	10.808	0.176	0.130	0.352	0.261	0.529	0.391

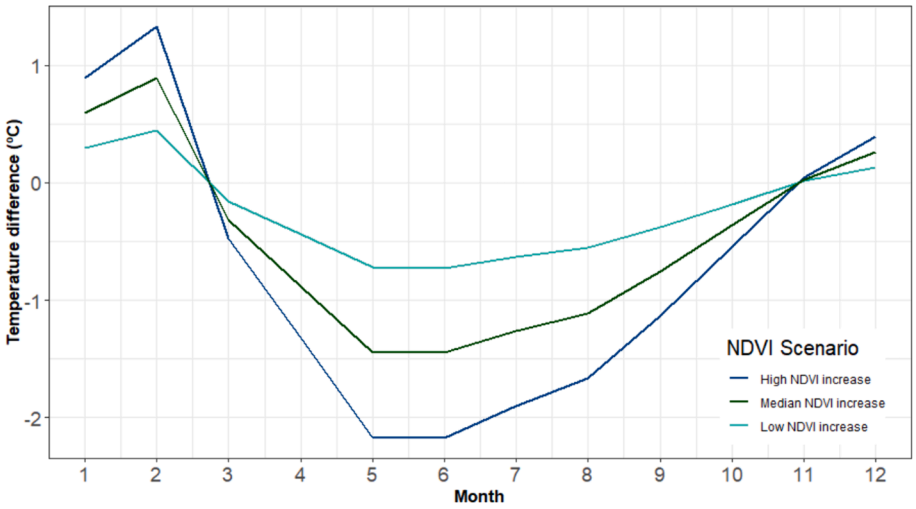

Fig. 8. Evolution in the AT difference for every month with respect to the reference weather data set in the 3 new NDVI scenarios: the Olivereta station.

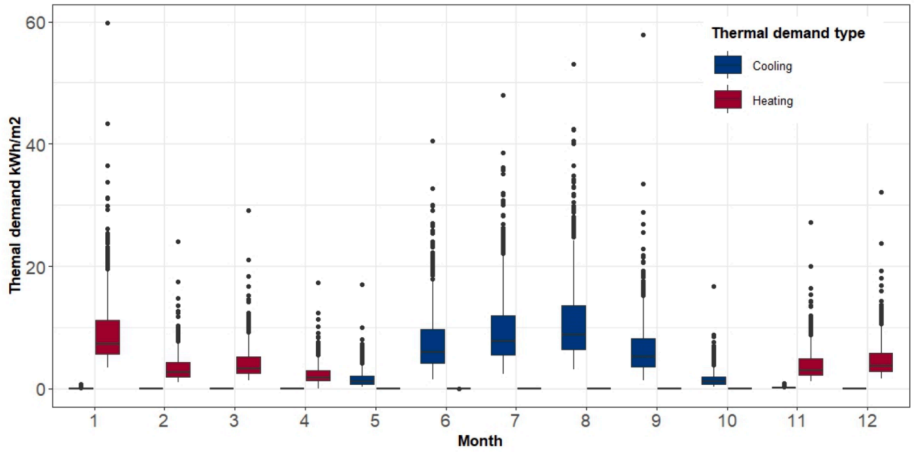

Fig. 9. Heating and cooling thermal demand distribution throughout the year for the 1000 buildings under study.

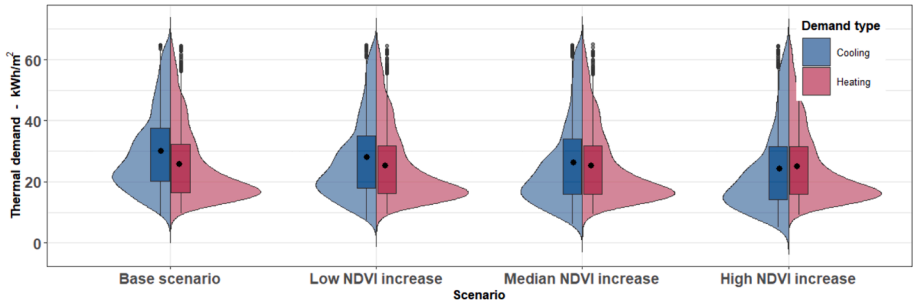

Fig. 10. Annual heating and cooling thermal demand for the base case and new scenarios.

the baseline case. The first graph, Fig. 11, shows the percentage reduction in electricity consumption for heating and cooling. This graph reveals a highly significant reduction in cooling, averaging 10 %, 20 %, and up to 30 % for the three scenarios, respectively. It is also evident that with more vegetation, there is greater dispersion in the results. Some buildings have obtained greater benefits from nature-based measures, of up to 40 % in their electricity consumption, while others barely show a change. These values are consistent with the results of the previous analyses found in [12–14].

Considering the limited increase in temperature, the expected savings as far as heating is concerned are under 5 % and the dispersion is almost non-existent, even in the best scenario. This is still a significant result because one assumption for the authors was that vegetation reduces the area's temperature, which is not a desirable effect in winter. However, the vegetation also prevents the heat generated by the city from being radiated outside, especially on the clear days so common in the Mediterranean winter. Hence, the study has shown that vegetation helps in both heating and cooling months, making it a valuable measure for the purposes of achieving energy efficiency and comfort throughout the year.

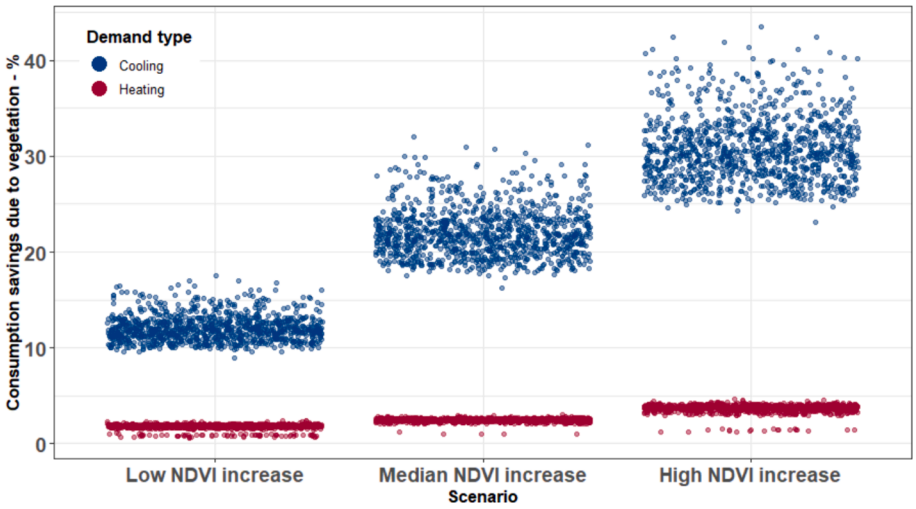

Fig. 11. Annual savings in heating and cooling consumption due to vegetation increase for the new NDVI scenarios.

It is important to remember here that studies such as [12] find that the absolute humidity of the city is positively correlated with the influence of the UHI effect on the energy demand of buildings. However, relative humidity and precipitation is insignificant in mediating the energy impacts of the UHI effect. In València, absolute humidity is quite high all year round, especially in the summer with typical values of 15 g/m3 [35].

The authors have generated new graphs with the aim of understanding the causes of result dispersion. Fig. 12 displays the annual savings in electricity consumption for the three scenarios, ordered according to the year of construction. This graph shows the reduction in relation to annual consumption, i.e., the older the building, the less influential the variations in NDVI, although the variation is very small. In addition, it can be observed that the maximum annual reduction achieved is around 17 % for the scenario with the highest vegetation values. For the other two scenarios, the average ranges between 6 % and 12 %, respectively. The points are grouped according to the registration date of each building; it was usual for older buildings to be registered upon periodic inspections, every 5 years, rather than when they were built. It is interesting to reiterate that each building has responded differently to the simulated measures, and there is great variability in the results. Given that each building has unique characteristics and shapes, it is important to consider them so as to improve the quality of the results.

Analysing the results from another perspective, Fig. 13 illustrates the annual savings in electricity consumption for every building, ordered according to their shape factor. This factor is calculated as the free surface of the building (the part in contact with the air, without being in contact with other buildings, elements, or the ground) divided by the internal volume to be conditioned. This parameter has been shown in multiple studies to correlate quite well with the building's energy needs. The figure reveals a clearer trend: the higher the exterior surface-to-volume ratio, the less effect these measures have. This can be understood as follows: the greater the surface area in contact with the air relative to the internal volume, the less effect changes in climate will have on consumption. In simpler terms, a greater exterior surface area leads to fewer benefits from nature-based solutions. A variation of 5–10 % can be considered for each scenario with respect to the maximum and minimum values. However, it would be interesting to explore further, in future studies, how other characteristic parameters of buildings correlate with the results of the study.

6. Conclusions

In a comprehensive overview of the challenges posed by climate change, the European Union's strategic focus on mitigation and

Fig. 12. Annual consumption savings due to increase in vegetation, arranged by construction year.

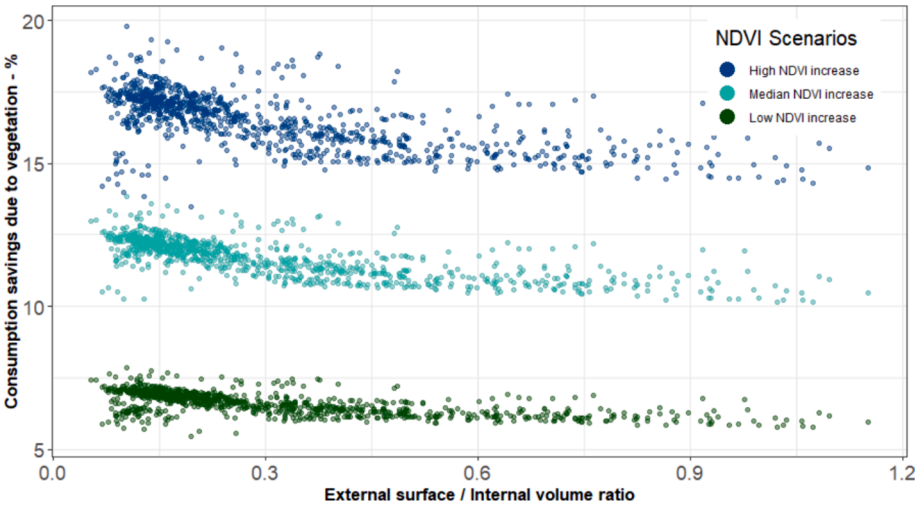

Fig. 13. Annual consumption savings due to vegetation increase, arranged according to shape factor.

adaptation policies gives a critical role to cities. The need for meticulous planning spanning various sectors, especially energy use in high-density urban areas, is highlighted as being essential if climate goals are to be achieved. The escalating frequency of extreme weather events and the European Union's ambitious targets for emissions reduction further underscore the urgency of implementing effective measures. Additionally, studies delve into the examination of urban microclimates, emphasizing the importance of understanding and addressing the areas most affected by global warming. Nature-based solutions, including green infrastructure and urban parks, are identified as potent tools for reducing energy demand and mitigating the urban heat island effect. For this purpose. satellite imagery, notably Landsat-8, plays a pivotal role in monitoring and quantifying these changes. The nuanced exploration of factors contributing to urban hot spots and the subsequent focus on surface temperature assessments using satellite data provide valuable insights into an understanding of the intricate dynamics of urban environments. This research assesses the impact of nature-based measures on the thermal demand of buildings in an urban area of València, on the Mediterranean coast of Spain. Through the analysis of land surface temperature data, vegetation levels, modified climate data files and thermal demand simulations, significant findings have been obtained, contributing to a comprehensive understanding of how vegetation influences the energy consumption of buildings. A clear correlation has been established between vegetation and land surface temperature. Landsat-8 satellite data facilitated this analysis, revealing a consistent influence of vegetation on temperature throughout the year. The study conducted a comprehensive temporal analysis, correlating the NDVI and LST for each month. The results indicated that vegetation has a notable impact on temperature, with distinct patterns observed in different seasons. This analysis provided insights into the dynamic nature of the relationship between vegetation and soil temperature.

Extending the analysis to include AT, the study explores the relationship between this parameter and LST. The comparison of temperatures from both sources, taken at the same locations and times, allows for the assessment of their correlation, which provides insights into how an increase in LST influences air temperature. By establishing a correlation between LST and AT, the study bridges the gap between surface temperature dynamics and their consequences for the overall atmospheric conditions. This nuanced analysis contributes to a more comprehensive perspective on the impact of urban vegetation on the local microclimate, thereby advancing the knowledge base for sustainable urban planning and climate-responsive building design.

The research incorporated the simulation of climate scenarios, introducing varying levels of vegetation. The results demonstrated not only a substantial reduction in cooling demand, particularly during the summer months, but also. the nuanced impact on heating demand, emphasizing the dual-season effectiveness of vegetation in moderating temperature extremes. The simulation of climate scenarios is a pivotal aspect of the research, enabling the assessment of how different levels of vegetation impact the heating and cooling needs of buildings. The significant reduction in cooling demand, primarily observed during the summer months, underscores the potential of nature-based solutions to mitigate the impact of the urban heat island effect. The focus on heating demand highlights the versatility of vegetation, influencing not only the warm season but also exerting a noticeable effect during the colder months. It should be remembered that absolute humidity is positively correlated with the influence of the UHI effect on the energy demand of buildings. In cities with lower absolute humidity influence of NDVI changes may be smaller.

An intriguing observation was the influence of the building shape factor, that is exterior surface-to-volume ratio, on the effectiveness of nature-based solutions. Buildings with a lower form factor exhibited a more pronounced reduction in energy consumption. Further analysis, considering the year of construction, revealed diverse responses of buildings to simulated measures. The annual savings in electricity consumption varied, with older buildings showcasing a range of outcomes. These findings underscore the need for tailored simulations that account for the unique characteristics of each building.

In conclusion, this study provides valuable insights into the complex interplay between vegetation, surface temperature, and building energy demand in urban environments. The findings show the potential of nature-based measures to mitigate energy consumption and enhance the resilience of urban areas to climate variability. Future research should explore additional building parameters to refine the understanding of the relationships observed in this study.

The limitations, and potential future lines of improvement of this study are: i) 2 satellite images are obtained per month, and when there are shadows (clouds) they are not useful. Other sources of information are needed to obtain more complete time series; ii)it would be better to be able to modify the climatic files day by day, not just month by month; iii) real data from weather stations are used, which can make extrapolation to other cities difficult; and finally, iv) this study could be replicated to many different Mediterranean cities to try to quantify the role that variables, such as absolute humidity, urban planning, city surroundings, etc. play in the impact of the UHI effect on building energy demand.

CRediT authorship contribution statement

C. Prades-Gil: Writing – original draft, Visualization, Validation,

Software, Resources, Methodology, Investigation, Formal analysis, Data curation, Conceptualization. **J.D. Viana-Fons:** Software, Methodology, Investigation, Conceptualization. **X. Masip:** Writing – review & editing, Conceptualization. **A. Cazorla-Marín:** Writing – review & editing, Supervision, Resources, Methodology, Formal analysis. **T. Gómez-Navarro:** Writing – review & editing, Supervision, Resources, Project administration, Conceptualization.

Declaration of competing interest

The authors declare that they have no known competing financial interests or personal relationships that could have appeared to influence the work reported in this paper.

Data availability

The authors do not have permission to share data.

Acknowledgments

This study has been possible thanks to the support of the Chair of Urban Energy Transition, UPV - Las Naves & València Clima i Energia and Grupo ImpactE planificación Urbana S.L. It was also supported by the project PURPOSED PID2021-128822OBI00, funded by MCIN/AEI/10.13039/501100011033/ and by FEDER - A way of doing Europe. In addition, the authors want to acknowledge the association AVAMET for providing the weather data used in this study as part of the collaboration agreement between AVAMET and UPV, significantly enhancing the robustness and representativeness of the results.

Appendix A. Date and time of satellite images.

Table 3. Date and time of each satellite image from Landsat-8 collected.

2014–01-20 10:38:34	2014–02-12 10:44:28	2014–03-16 10:44:06	2014–04-10 10:37:31	2014–05-03 10:43:18	2014–05-19 10:43:08	2014–06-04 10:43:15	2014–07-22 10:43:29
2014–09-01 10:37:32	2014–10-10 10:43:49	2014–12-06 10:37:35	2014–12-29 10:43:40	2015–01-14 10:43:39	2015–01-30 10:43:34	2015–02-08 10:37:19	2015–10-22 10:37:30
2015–03-12 10:37:02	2015–04-20 10:42:59	2015–05-15 10:36:26	2015–06-07 10:42:25	2015–08-03 10:37:03	2015–09-20 10:37:24	2015–11-30 10:43:46	2019–01-02 10:37:18
2019–02-26 10:43:18	2019–03-14 10:43:12	2019–05-26 10:37:07	2019–06-18 10:43:27	2019–07-04 10:43:32	2019–07-29 10:37:28	2019–08-14 10:37:34	2019–09-22 10:43:55
2019–10-01 10:37:47	2019–10-17 10:37:49	2019–11-18 10:37:46	2019–12-27 10:43:51	2020–01-05 10:37:38	2020–01-12 10:43:48	2020–02-06 10:37:29	2020–02-29 10:43:35
2020–05-03 10:43:03	2020–05-19 10:43:03	2020–06-13 10:37:04	2020–06-20 10:43:18	2020–07-06 10:43:26	2020–07-31 10:37:22	2020–08-07 10:43:35	2020–10-26 10:43:56
2020–11-11 10:43:53	2020–11-20 10:37:45	2020–12-13 10:43:58	2020–12-22 10:37:45	2020–12-29 10:43:54	2021–01-14 10:43:47	2021–01-30 10:43:45	2021–03-12 10:37:19
2021–04-20 10:43:16	2021–05-06 10:43:06	2021–06-07 10:43:24	2021–07-18 10:37:22	2021–09-27 10:43:57	2021–11-07 10:37:50	2021–11-30 10:43:58	2021–12-09 10:37:47
2022–01-17 10:43:49	2022–02-02 10:43:45	2022–04-07 10:43:24	2022–05-09 10:43:30	2022–06-10 10:43:44	2022–07-12 10:43:50	2022–08-06 10:37:54	2022–09-07 10:38:00
2022–09-30 10:44:15	2022–10-25 10:38:03	2022–11-10 10:38:02	2022–12-28 10:37:50	2023–01-04 10:44:01	2023–01-20 10:43:55	2023–02-05 10:43:35	2023–03-25 10:43:27
2023–04-03 10:37:10	2023–05-05 10:36:51	2023–06-06 10:36:48	2023–07-08 10:37:07	2023–07-15 10:43:19	2023–08-09 10:37:17	2023–08-25 10:37:26	2023–09-01 10:43:36
2023–09-26 10:37:32	2023–10-12 10:37:36						

Appendix B. : NDVI and LST comparison graphs.

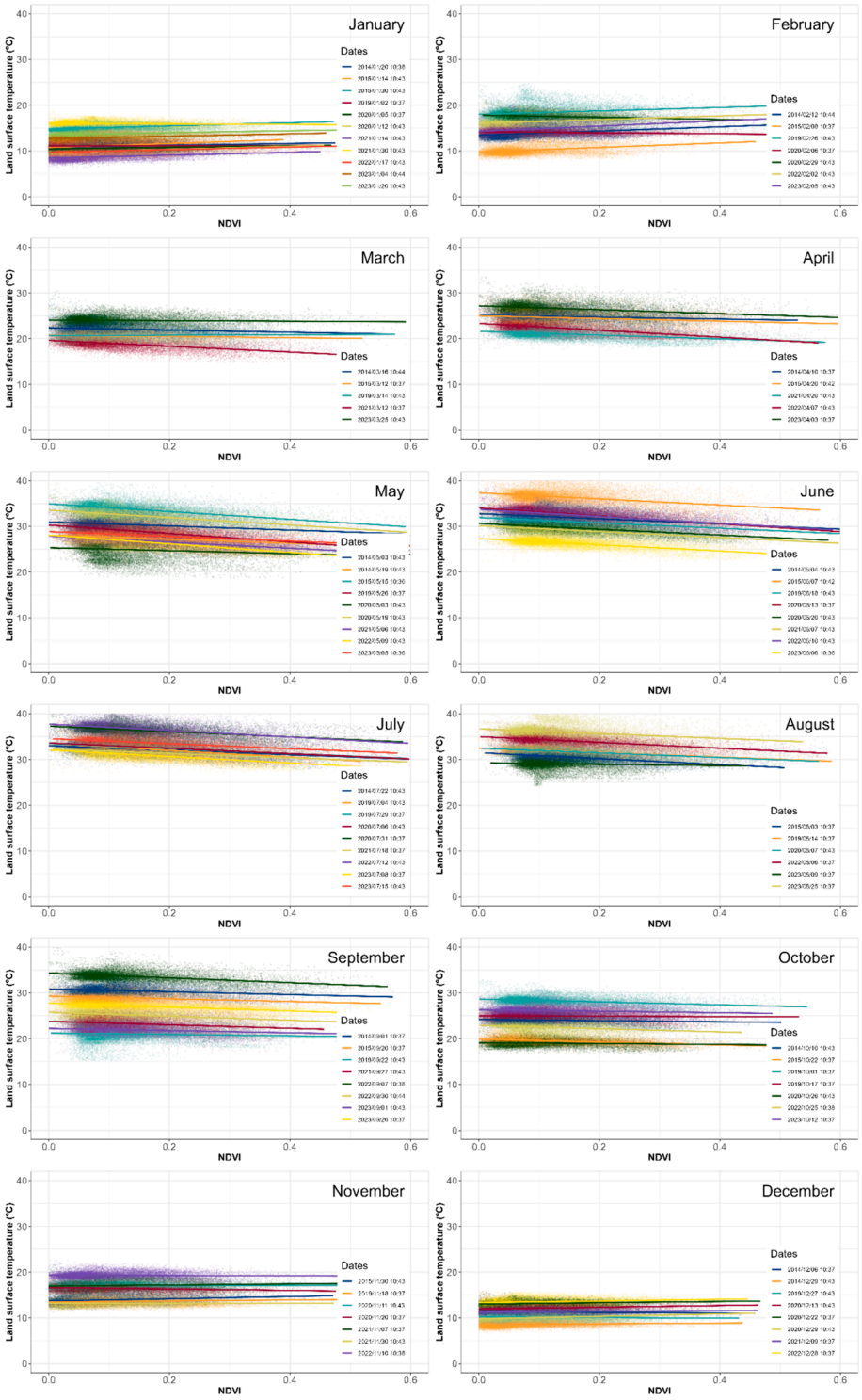

Fig. 14. Relationship between NDVI and LST for each Landsat-8 image, organized according to months.

Appendix C. : Constructive information from the study sample.

The sample of buildings used in the simulation of the present article are the same as those used in article [43]. The following graphs have been compiled from article [43].

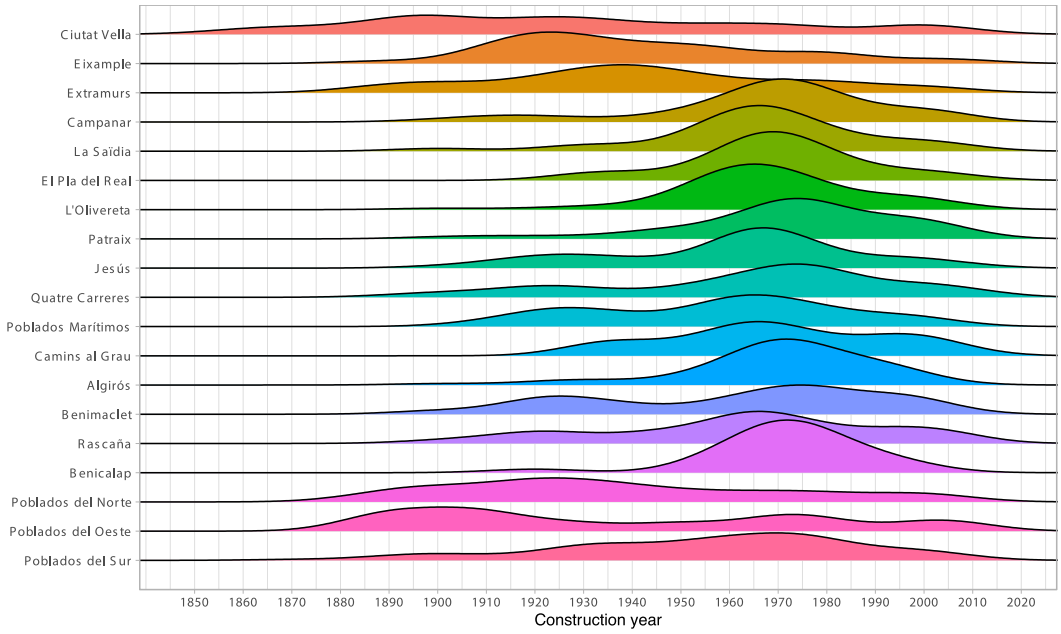

Fig. 15. Distribution of buildings by the period of construction for the 19 districts of València.

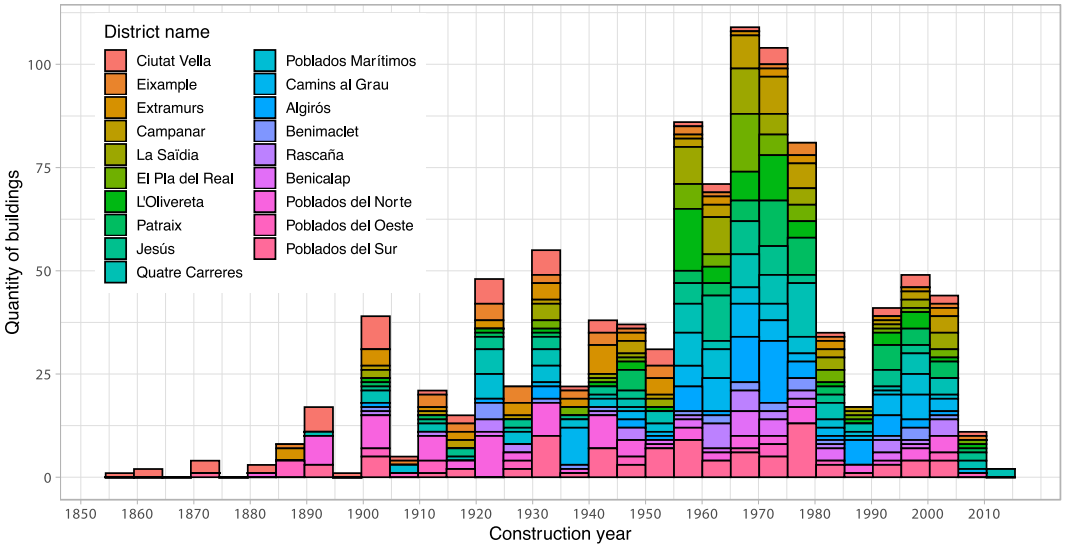

Fig. 16. Buildings studied in the present research, grouped by construction year and district.

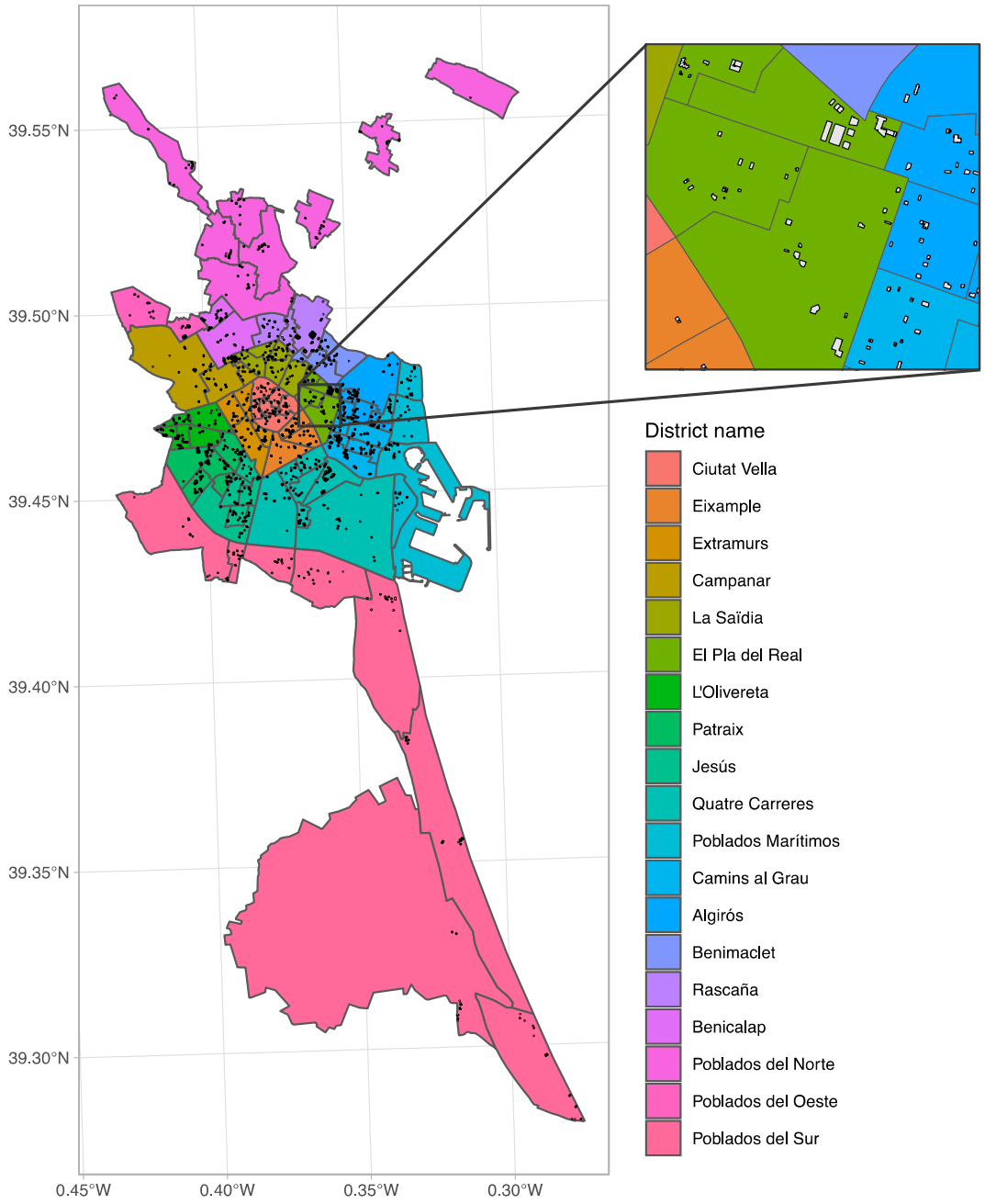

Fig. 17. Spatial representation of the studied buildings in the research, located in the city of València.

References

[1] European Commission, "Proposed Mission: 100 Climate-neutral Cities by 2030 – by and for the Citizens. Report of the Mission Board for climate-neutral and smart cities," 2020. doi: 10.2777/62649.

[2] World Urbanization Prospects, "The World 's Cities in 2018," 2018.

[3] O'Neill BC, et al. The Scenario Model Intercomparison Project (ScenarioMIP) for CMIP6. Geosci Model Dev 2016;9(9):3461–82. https://doi.org/10.5194/gmd-9-3461-2016.

[4] European Commission, "Going climate-neutral by 2050," p. 20, 2019.

[5] European Commission, "The roadmap for transforming the EU into a competitive, low-carbon economy by 2050," pp. 1–4, 2011.

[6] Perera ATD, Nik VM, Chen D, Scartezzini JL, Hong T. Quantifying the impacts of climate change and extreme climate events on energy systems. Nat Energy 2020;5(2):150–9. https://doi.org/10.1038/s41560-020-0558-0.

[7] C. Calice, C. Clemente, A. Salvati, M. Palme, and L. Inostroza, "Urban Heat Island effect on the energy consumption of institutional buildings in Rome," *iopscience.iop.org*, doi: 10.1088/1757-899X/245/8/082015.

[8] Langemeyer J, Wedgwood D, McPhearson T, Baró F, Madsen AL, Barton DN. Creating urban green infrastructure where it is needed – A spatial ecosystem service-based decision analysis of green roofs in Barcelona. Sci Total Environ 2020;707. https://doi.org/10.1016/j.scitotenv.2019.135487.

[9] Benedito Durà V, Meseguer E, Hernández Crespo C, Martín Monerris M, Andrés Doménech I, Rodrigo Santamalia ME. Contribution of green roofs to urban arthropod biodiversity in a Mediterranean climate: A case study in València, Spain. Build Environ 2023;228:109865. https://doi.org/10.1016/J.BUILDENV.2022.109865.

[10] Iungman T, et al. Cooling cities through urban green infrastructure: a health impact assessment of European cities. Lancet 2023. https://doi.org/10.1016/S0140-6736(22)02585-5.

[11] I. Anguelovski *et al.*, "Green gentrification in European and North American cities", doi: 10.1038/s41467-022-31572-1.

[12] Singh M, Sharston R. Quantifying the dualistic nature of urban heat Island effect (UHI) on building energy consumption. Energy Build 2022;255. https://doi.org/10.1016/j.enbuild.2021.111649.
[13] T. O.-Q. journal of the royal meteorological society and undefined 1982, "The energetic basis of the urban heat island," *patarnott.comTR OkeQuarterly journal of the royal meteorological society, 1982•patarnott.com*, vol. 108, no. 455, p. 551, 1982, Accessed: Dec. 03, 2023. [Online]. Available: https://www.patarnott.com/pdf/Oake1982_UHI.pdf.
[14] A. A.-I. J. of C. a J. of and undefined 2003, "Two decades of urban climate research: a review of turbulence, exchanges of energy and water, and the urban heat island," *Wiley Online LibraryAJ ArnfieldInternational Journal of Climatology: a Journal of the Royal, 2003•Wiley Online Library*, vol. 23, no. 1, pp. 1–26, Jan. 2003, doi: 10.1002/joc.859.
[15] Grigoraș G, Urițescu B. Land Use/Land Cover changes dynamics and their effects on Surface Urban Heat Island in Bucharest, Romania. Int J Appl Earth Obs Geoinf 2019;80:115–26. https://doi.org/10.1016/j.jag.2019.03.009.
[16] Konarska J, Klingberg J, Lindberg F. Applications of dual-wavelength hemispherical photography in urban climatology and urban forestry. Urban for Urban Green 2021;58. https://doi.org/10.1016/J.UFUG.2020.126964.
[17] Wahba SM, Kamel BA, Nassar KM, Abdelsalam AS. Effectiveness of green roofs and green walls on energy consumption and indoor comfort in arid climates. Civil Eng J 2018;4(10):2284. https://doi.org/10.28991/cej-03091158.
[18] Vox G, Blanco I, Schettini E. Green façades to control wall surface temperature in buildings. Build Environ 2018;129:154–66. https://doi.org/10.1016/j.buildenv.2017.12.002.
[19] Davis MM, Vallejo Espinosa AL, Ramirez FR. Beyond green façades: active air-cooling vertical gardens. Smart Sustain Built Environ 2019;8(3):243–52. https://doi.org/10.1108/SASBE-05-2018-0026.
[20] Sari NM, Rokhmatuloh R, Manessa MDM. Monitoring dynamics of vegetation cover with the integration of OBIA and random forest classifier using sentinel-2 multitemporal satellite imagery. Geoplan J Geomat Plann 2021;8(2). https://doi.org/10.14710/geoplanning.8.2.75-84.
[21] Özyavuz M. Analysis of changes in vegetation using multitemporal satellite imagery, the case of Tekirdağ Coastal Town. J Coast Res 2010;26(6):1038–46. https://doi.org/10.2112/JCOASTRES-D-10-00030.1.
[22] Al-Kindi KM, Al Nadhairi R, Al Akhzami S. dynamic change in normalised vegetation index (NDVI) from 2015 to 2021 in Dhofar, Southern Oman in response to the climate change. Agriculture 2023;13(3). https://doi.org/10.3390/agriculture13030592.
[23] Lee G, Hwang J, Cho S. A novel index to detect vegetation in urban areas using UAV-based multispectral images. App Sci 2021;11(8). https://doi.org/10.3390/app11083472.
[24] Zhao Y, Hou P, Jiang J, Zhao J, Chen Y, Zhai J. High-spatial-resolution NDVI reconstruction with GA-ANN. Sensors 2023;23(4). https://doi.org/10.3390/s23042040.
[25] Heaviside C, Macintyre H, Vardoulakis S. The urban heat island: implications for health in a changing environment. Curr Environ Health Rep 2017;4(3):296–305. https://doi.org/10.1007/s40572-017-0150-3.
[26] Ngie A, Abutaleb K, Ahmed F, Darwish A, Ahmed M. Assessment of urban heat island using satellite remotely sensed imagery: a review. S Afr Geogr J Jul. 2014;96(2):198–214. https://doi.org/10.1080/03736245.2014.924864.
[27] Kim D, Yu J, Yoon J, Jeon S, Son S. Comparison of accuracy of surface temperature images from unmanned aerial vehicle and satellite for precise thermal environment monitoring of urban parks using in situ data. Remote Sens (Basel) 2021;13(10). https://doi.org/10.3390/rs13101977.
[28] H. Yang *et al.*, "Measuring the Urban Land Surface Temperature Variations Under Zhengzhou City Expansion Using Landsat-Like Data," 2020. doi: 10.3390/rs12050801.
[29] Tan K, Liao Z, Du P, Wu L. Land surface temperature retrieval from Landsat 8 data and validation with geosensor network. Front Earth Sci 2017;11(1):20–34. https://doi.org/10.1007/s11707-016-0570-7.
[30] Masson V, et al. City-descriptive input data for urban climate models: Model requirements, data sources and challenges. Elsevier B.V.; 2020. doi: 10.1016/j.uclim.2019.100536.
[31] G. Lobaccaro, K. De Ridder, J. Acero, H. H.- Sustainability, and undefined 2021, "Applications of models and tools for mesoscale and microscale thermal analysis in mid-latitude climate regions—A review," *mdpi.com*, 2021, Accessed: Jan. 28, 2023. [Online]. Available: https://www.mdpi.com/1351192.
[32] G. Kaplan, U. Avdan, Z. A.-M. D. Publishing, and undefined 2018, "Urban heat island analysis using the landsat 8 satellite data: A case study in Skopje, Macedonia," *mdpi.com*, 2018, doi: 10.3390/ecrs-2-05171.
[33] Montaner-Fernández D, et al. Spatio-temporal variation of the urban heat island in Santiago, Chile during summers 2005–2017. Remote Sens (basel) 2020;12(20):1–19. https://doi.org/10.3390/rs12203345.
[34] Yang C, Yan F, Zhang S. Comparison of land surface and air temperatures for quantifying summer and winter urban heat island in a snow climate city. J Environ Manage 2020;265. https://doi.org/10.1016/j.jenvman.2020.110563.
[35] AEMET, "Normal climatological values. Valencia, Spain," https://www.aemet.es/es/serviciosclimaticos/datosclimatologicos/valoresclimatologicos?l=8416&k=val.
[36] "Institut Cartogràfic Valencià - ICV - Generalitat Valenciana." Accessed: Jul. 29, 2024. [Online]. Available: https://icv.gva.es/es/.
[37] "AVAMET Associació Valenciana de Meteorologia." Accessed: Dec. 07, 2023. [Online]. Available: https://www.avamet.org/.
[38] "Agencia Estatal de Meteorología - AEMET. Gobierno de España." Accessed: Dec. 07, 2023. [Online]. Available: https://www.aemet.es/es/portada.
[39] Roy DP, et al. Landsat-8: Science and product vision for terrestrial global change research. Remote Sens Environ 2014;145(December 2018):154–72. https://doi.org/10.1016/j.rse.2014.02.001.
[40] Jimenez-Munoz JC, Sobrino JA, Skokovic D, Mattar C, Cristobal J. Land surface temperature retrieval methods from landsat-8 thermal infrared sensor data. IEEE Geosci Remote Sens Lett 2014;11(10):1840–3. https://doi.org/10.1109/LGRS.2014.2312032.
[41] Department of the Interior U.S. Geological Survey, "Landsat 8 (L8) Data Users Handbook," 2019.
[42] Prades-Gil C, Viana-Fons JD, Masip X, Cazorla-Marín A, Gómez-Navarro T. An agile heating and cooling energy demand model for residential buildings. Case study in a mediterranean city residential sector. Renew Sustain Energy Rev 2023;175:113166. https://doi.org/10.1016/J.RSER.2023.113166.
[43] Bruno R, Bevilacqua P, Arcuri N. Assessing cooling energy demands with the EN ISO 52016–1 quasi-steady approach in the Mediterranean area. J Build Eng 2019;24:100740. https://doi.org/10.1016/j.jobe.2019.100740.
[44] Loga T, Stein B, Diefenbach N. TABULA building typologies in 20 European countries—Making energy-related features of residential building stocks comparable. Energy Build 2016;132:4–12. https://doi.org/10.1016/j.enbuild.2016.06.094.
[45] M. Febrero, "PRESTACIONES MEDIAS ESTACIONALES DE LAS BOMBAS DE CALOR PARA PRODUCCIÓN DE CALOR EN EDIFICIOS," 2014.
[46] Grigoraș G, Urițescu B. Land use/land cover changes dynamics and their effects on surface urban heat island in Bucharest, Romania. Int J Appl Earth Obs Geoinf 2019;80:115–26. https://doi.org/10.1016/J.JAG.2019.03.009.